arXiv:1401.5932v1 [cond-mat.soft] 23 Jan 2014

Mixing and segregation of ring polymers: spatial confinement and molecular crowding effects

Jaeoh Shin [†], Andrey G. Cherstvy[†], and Ralf Metzler[†,♯,1]

[†]Institute for Physics & Astronomy, University of Potsdam, 14476 Potsdam-Golm, Germany

[♯]Department of Physics, Tampere University of Technology, 33101 Tampere, Finland

E-mail: [1]rmetzler@uni-potsdam.de

Abstract. During the life cycle of bacterial cells the non-mixing of the two ring-shaped daughter genomes is an important prerequisite for the cell division process. Mimicking the environments inside highly crowded biological cells, we study the dynamics and statistical behaviour of two flexible ring polymers in the presence of cylindrical confinement and crowding molecules. From extensive computer simulations we determine the degree of ring-ring overlap and the number of inter-monomer contacts for varying volume fractions ϕ of crowders. We also examine the entropic de-mixing of polymer rings in the presence of mobile crowders and determine the characteristic times of the internal polymer dynamics. Effects of the ring length on ring-ring overlap are also analysed. In particular, on systematic variation of the fraction of crowding molecules a $(1-\phi)$-scaling is found for the ring-ring overlap length along the cylinder axis, and a non-monotonic dependence of the 3D ring-ring contact number is predicted. Our results help to rationalise the implications of macromolecular crowding for circular DNA molecules in confined spaces inside bacteria as well as in localised cellular compartments inside eukaryotic cells.

PACS numbers: 87.15.A-, 36.20.Ey

1. Introduction

The physical effects of spatial confinement on the properties of ring polymers is important to the physical understanding of the entropy-driven segregation of the two bacterial daughter chromosomes upon cell division [1] and the structure of eukaryotic metaphase chromosomes [2, 3, 4]. For rod-like bacteria cells such as *E. coli*, *Bacillus subtilis*, or *streptobacillus* a directed motion and segregation of duplicated chromosomes along the cell axis is detected after DNA replication, see, for instance, Ref. [5]. In eukaryotes, upon decondensation of the chromosomes in a strongly limited space inside the nucleus, the existence of chromosomal territories [6, 7] indicates an ultra-slow polymer mixing dynamics [8, 9, 10, 11]. Knotting of DNA molecules in tight spaces inside viral capsids another example of external polymer confinement in biology [12, 13]. *In*

vitro, the elongation and compaction of long DNA molecules confined in nano-channels upon increasing fraction of the crowding agent was indeed detected [14].

Internal polymer confinement *in vivo* is due to macromolecular crowding, which enforces DNA condensation in bacterial cells [15, 16] where the volume fraction occupied by crowding macromolecules such as RNA, ribosomes, or other biomacromolecules reaches $\phi = 30 \ldots 35\%$ [17]. The abundance of crowding agents effects a viscoelastic environment [18, 19] that severely alters the diffusional dynamics of endogeneous cytoplasmic granules and of submicron tracers inside living cells [20, 21, 22, 23, 24, 25]. Concurrently the internal dynamics of polymers and the macromolecular association kinetics inside biological cells are dramatically changed [26, 27, 28]. The effect of various polymeric crowders on the opening-closing dynamics of DNA hairpins has recently been experimentally probed in Ref. [29]. Crowding can also facilitate phase separation and compartmentalisation of the bacterial cytoplasm. In theoretical models, inert spherical obstacles are often used to mimic highly crowded interiors of bacterial [17] and eukaryotic [30] cells. Crowding particles cause effective interactions between the polymer segments of the same chain and between the two chains in confinement, as studied in the present paper.

From the theoretical perspective, overlapped segments of long polymer chains experience entropic repulsion scaling with the number of overlapping polymer blobs [31]. In a dense polymer melt the entanglements of the chains also slow down the polymer dynamics [32, 33]. In the presence of obstacles, the extension and dynamics of ring polymers on the lattice was analysed in Refs. [34].

A number of simulations studies of polymers under external confinement in various geometries appeared in the literature in recent years [35, 36, 37, 38, 40, 41]. In particular, the size scaling of ring polymers in dense melts was analysed by computer simulations in Ref. [41]. As the concentration of rings c grows and the effective volume available for their expansion decreases, the scaling exponent for the radius of gyration $\langle R_g^2 \rangle \simeq n^{2\nu}$ decreases from $\nu = 3/5$ to $\nu \approx 0.3$, mirroring impeded polymer extension. Neighbouring rings in dense melts thus induce a spherical caging effect, and their dimension was shown to scale as $\langle R_g^2 \rangle \sim c^{-0.59}$ in terms of the ring concentration [41]. The segregation of semi-flexible macromolecules in nano-channels was shown theoretically in Ref. [42]. Ring polymers in confinement were successfully used to model the bacterial chromosome [38] and to rationalise the implications of supercoiling for the contact maps of eukaryotic interphase chromosomes [39].

More specific with respect to our present study, the entanglement propensity of ring and linear polymers under external cylindrical confinement with respect to the phenomenon of DNA homologous recombination were analysed recently in Ref. [43]. It was shown that linear chains penetrate into one another significantly easier than ring polymers. Finally, the threading of ring polymers inside a polymer gel was recently studied by simulations [44].

The statistical properties of linear and ring polymers in the presence of crowding effects were considered in a number of theoretical and simulations studies. In particular,

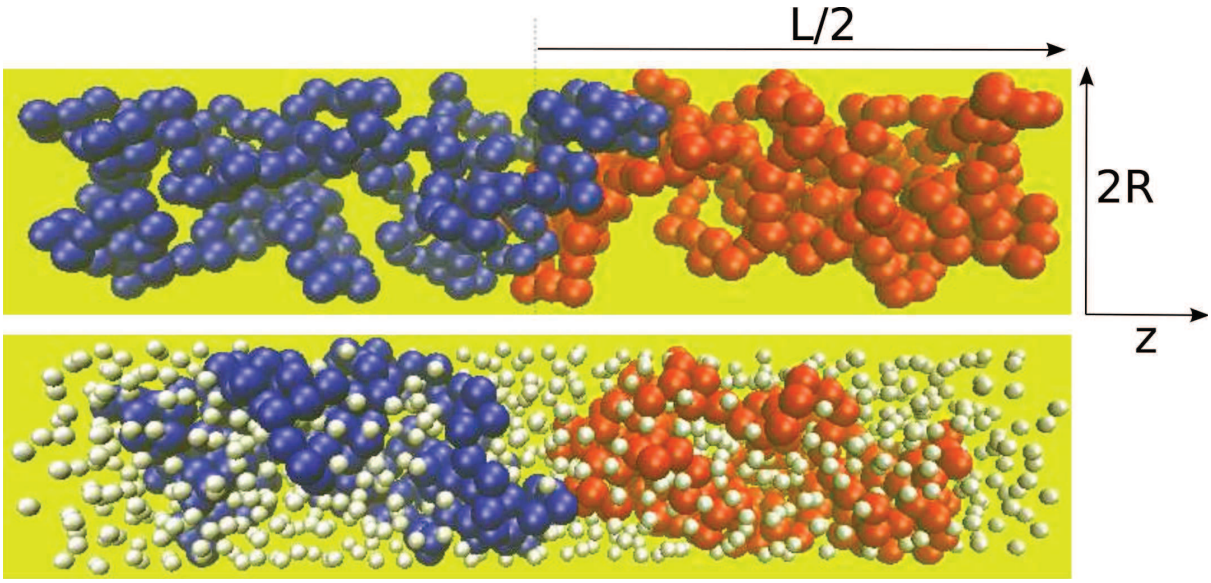

Figure 1. Typical conformations of two polymer rings (rendered in red and blue, respectively) in a cylindrical confinement. Parameters: the rings are $n = 200$ monomers long, the cylinder radius is $R = 4.5\sigma$ in terms of the monomer size σ, with the fraction of crowders $\phi = 0$ (top) and $\phi = 0.182$ (bottom). Crowding particles, which are equal in size to the chain monomers, are shown in this image in light-yellow colour with 1/2 of their actual radius, to improve the visibility of the image.

the behaviour of single knotted polymer rings on a regular lattice of obstacles was simulated in Refs. [45, 46]. For random-loop and self-avoiding polymers in the presence of crowding the computer modelling in Refs. [47, 48] was shown to give rise to a non-monotonic dependence of $\langle R_g^2 \rangle$ on the volume fraction occupied by the crowders, ϕ, featuring a slight minimum in the chain dimensions at $\phi \approx 0.2$. Related to this, the rates of chemical diffusion-limited reactions in molecularly crowded media in confined environments was shown to reveal a maximum at $\phi \approx 0.2$ [49].

In a biophysical context, the effect of crowding on gene regulation was studied with respect to facilitated diffusion and target search on DNA by DNA-binding proteins in Refs. [28, 50]. The translocation of polymers between the two reservoirs with crowders of equal [51] and non-equal [52] sizes has also been rationalised by simulations. The implications of crowding environments inside nano-channels have also been recently

examined by simulations [53]. Finally, the effects of crowders on the looping probabilities of polymer chains in the presence of external confinement and molecular crowding is also important [54].

Below, we take a step further and analyse the joint effect of external confinement and internal crowding for two unknotted ring polymers in a model rod-shaped bacteria. More concretely, we perform molecular dynamics simulations for two polymer rings confined in a cylindric volume in the presence of mobile crowders, which are subject to the same thermal bath, as illustrated in Fig. 1. We analyse how the entropic repulsion of these thermally agitated ring polymers becomes altered under these crowding conditions.

The paper is organised as follows. In the next Section, we present the details of the simulations model. In Section 3 we rationalise the effects of external cylindrical confinement and internal confinement by the crowding obstacles. The main results for the static properties of the mutual overlap of the polymer rings and their dynamic characteristics are presented. In Section 4 we discuss the basic results and their implications to the biological system and with respect to polymer physics.

2. Model and implementation of the simulations

2.1. Polymer chains

The standard finitely extensible non-elastic (FENE) potential is used to model the interactions between the monomers in our polymer chains in the bead-spring coarse-grained model of the DNA molecule, namely,

$$U_{\rm FENE}(r) = -\frac{k}{2} r_{\rm max}^2 \ln\left(1 - \frac{r^2}{r_{\rm max}^2}\right). \tag{1}$$

Here k is the spring constant acting between nearest-neighbour beads and $r_{\rm max}$ is the maximum allowed separation between neighbouring monomers. The total number of monomers in the ring polymers varies in the simulations in the range $n = 60 \ldots 350$. Excluded-volume interactions between the polymer segments are introduced by the truncated Lennard-Jones repulsion (Weeks-Chandler-Andersen potential), that is,

$$U_{\rm LJ}(r) = \begin{cases} 4\epsilon[(\sigma/r)^{12} - (\sigma/r)^6] + \epsilon, & r < 2^{1/6}\sigma \\ 0, & \text{otherwise} \end{cases} \tag{2}$$

We here introduced the monomer-monomer distance r, σ is the monomer diameter, and ϵ is the strength of the potential. We set $k = 30$, $r_{\rm max} = 1.5\sigma$, and $\epsilon = 1$, where all energies are measured in units of the thermal energy $k_B T$, and distances are measured in units of σ. Analogous repulsive 6-12 Lennard-Jones potentials parameterise the chain-obstacle, chain-wall, and crowder-wall contact interactions. Along the axial z coordinate in our cylindrical geometry a harmonic potential is applied once a monomer attempts to move outside of the cylinder at $z < 0$ or $z > L$.

The dynamics of the position $\mathbf{r}_i(t)$ of the ith monomer in a polymer chain is described by the Langevin equation

$$m\frac{d^2\mathbf{r}_i(t)}{dt^2} = -\sum_{j=1,j\neq i}^{n}\nabla[U_{\rm LJ}(\mathbf{r}_i-\mathbf{r}_j)+U_{\rm FENE}(\mathbf{r}_i-\mathbf{r}_j)] - \sum_{j=1}^{N_{cr}}\nabla U_{\rm LJ}(\mathbf{r}_i-\mathbf{r}_{cr,j}) - \nabla U_{\rm LJ}(\mathbf{r}_i-\mathbf{R}_{\rm cyl}) - \xi\mathbf{v}_i(t)+\mathbf{F}(t). \quad (3)$$

Here m is the monomer mass, ξ is the friction coefficient, v_i is the monomer velocity, and $F(t)$ represents Gaussian delta-correlated noise with δ-correlations $\langle F(t)F(t')\rangle = 6\xi\delta(t-t')$. Similar Langevin equations are used for the dynamics of the positions $\mathbf{r}_{cr,j}$ of the crowding molecules in the presence of the confining cylinder at $\mathbf{R}_{\rm cyl}$. Similarly to the procedure described in Ref. [55], we implement the velocity Verlet algorithm with the characteristic integration time-step of $\Delta t = 0.01$.

The monomer size is set to $\sigma = 4$ nm determining the chain thickness that stays constant for different ring lengths simulated below. This thickness represents the effective physical DNA diameter including hydration water shells and electrostatic effects [56]. Our approach thus differs from that taken in Ref. [43], where the mixing of ring polymers of different lengths without a crowding agent was studied and the polymers were assumed to become thinner as they get longer. This assumption was used in Ref. [43] to keep a constant volume fraction ϕ_p of the polymer chains V_p in the simulation box of volume V, and it is estimated that

$$\phi_p = \frac{\text{DNA volume}}{\textit{E. Coli} \text{ volume}} = \frac{V_p}{V} \sim 1\ldots 5, \quad (4)$$

depending on the DNA thickness (the bare DNA diameter plus the electrostatic repulsive salt-dependent shell around it). We present the ring-ring contact number and overlap distance of rings for the fixed ϕ_p in Fig. 13.

The equilibration time of the polymer rings in our simulations depends on their length, the cell cylinder radius R, and the volume fraction ϕ of crowding particles in the simulation box. For typical parameters of the ring length

$$l = n\sigma \sim 200\sigma \quad (5)$$

and $R = 4.5\sigma$ used in simulations below, the chains equilibrate after $\sim 4\times 10^6$ simulation steps in the absence of crowders. The ring equilibration time grows with the chain length, and longer measurement times are required in order to sample the conformations of the polymer chains. The equilibration time also grows with the volume fraction ϕ of crowders due to the slow-down of the polymer dynamics, see below.

2.2. Crowding and confinement

We distinguish two types of volume confinement for the polymer chains: external confinement by the cylindrical cell walls and internal confinement by mobile crowding obstacles. The model cell in our simulations is represented by an impenetrable cylinder of length $L = 35\sigma$ and radius $R = 3.5\sigma\ldots 5.5\sigma$.

By the internal confinement we mimic the highly poly-disperse soup of various proteins, RNA, cytoskeletal elements, and organelles in the cell cytoplasm. The crowders in the bacterial cytoplasm have an average molecular weight of MW $\approx 40 \ldots 67$ kDa and diameter of $4 \ldots 8$ nm [47]. We neglect here the poly-dispersity in crowder sizes observed in real cells [57] and for simplicity assign to the crowders the same size $\sigma_{cr} = \sigma$ as for the chain monomers. The crowders are simulated as spherical particles of unit mass (similarly to the polymer bead), with systematically varying volume occupancy ϕ. Each polymer monomer therefore corresponds to ≈ 12 base pairs of the double-stranded DNA and MW $\approx 12 \times 0.66$ kDa. Every step in our simulations then corresponds to a real time of $\tau_0 = \sigma\sqrt{12 \times 660 \text{ Da}/(k_B T)} \approx 0.23$ ns. Simulating the crowders as particles with the more realistic value of MW of 67 kDa will slow down the crowder and polymer dynamics, renormalising the elementary simulation time unit to $\tau_0 \approx 0.66$ ns.

Varying the volume fraction of crowders in the simulations in the range $0 < \phi \lesssim 0.3$ we mimic the response of a cell to the changes in external osmolarity, exerting a pressure on the outer cell membrane causing dehydration (osmotic upshift) [58]. This volume fraction is computed per free solution volume, i.e.,

$$\phi = \frac{V_{cr}}{V - V_p} = \frac{N_{cr} v}{\pi R^2 L - n v}, \tag{6}$$

where $v = 4\pi(\sigma/2)^3/3$ is the volume of one chain monomer or of one crowding particle and N_{cr} is the number of crowding particles in the box. For the chain length $n = 200$ and cell length $L = 35\sigma$ the volume fraction of the two polymer rings is $\phi_p \approx 0.155$, 0.094, and 0.063 (close to the DNA crowding in *E.coli* [43]) for the respective cylinder radii $R = 3.5\sigma$, 4.5σ, and 5.5σ.

We consider only excluded volume interactions according to the above-mentioned interaction potentials and neglect other interactions within the ring polymers, including electrostatic interactions. The latter can be of importance for tightly bent and circular DNAs, particularly at low-salt, weak-screening conditions [59, 60, 61]. Our model also neglects effects of hydrodynamic interactions (both for rings and crowders) [62, 63], which can alter short-time polymer dynamics [64], but should not affect the static overlap properties of the rings. Polymer relaxation under confinement with and without hydrodynamic interactions was studied by computer simulations [65]. For the relaxation time τ_R of a polymer ring consisting of n monomers in a long cylindrical pore of radius R the relation $\tau_R \sim n^2 R^{0.9}$ was predicted [38, 65].

2.3. Ring contacts and decay of correlations

For each simulation step t we determine the number of contacts $N_{AB}(t)$ between the two ring polymers as follows. Each monomer is surrounded by a sphere with contact radius $r_c = 1.25 \ldots 2\sigma$ that defines the overlap volume. If the centre of mass of a monomer of another chain stays within this contact sphere for the contact time t_c, the contact is recorded as established. The time t_c is a measure of the internal dynamics of two intermingled rings. Within this time scale, the change in distances between contacting

monomers should be smaller than r_c. This validates the choice of the temporal and spacial thresholds for counting the number N_{AB} of ring-ring contacts.

The distance r_c represents the 'radius of action' within which the monomers are supposed to be involved in some physical interactions. For the DNA, this can be electrostatic or protein-mediated inter-molecular contacts [66]. Clearly, the results of counting the number N_{AB} of contacts depends on the threshold distance r_c (for comparison, the choice of $r_c = 1.5\sigma$ was used in Ref. [43]). We analyse the dependence of the contact number on the contact distance r_c in Fig. 11 below.

The average $\langle N_{AB} \rangle$ is computed via averaging over various polymer configurations after the system reached its equilibrium. The contact volume V_{AB} of the rings is estimated as $\langle N_{AB} \rangle$ multiplied by $\sim 1/2$ of the volume of the contact sphere, $\langle V_{AB} \rangle \approx \langle N_{AB} \rangle \, 4\pi (r_c/2)^3/3$. In addition to the three-dimensional inter-chain contact probability, scaling with $\langle N_{AB} \rangle$, we compute the one-dimensional mutual overlap length of two rings along the $z-$axis of the confining cylinder, $\langle l_{AB} \rangle$.

Note that we consider only torsionally relaxed rings, with no effects of super-coiling. The latter would result in more branched and topologically complex polymer structures, likely with more extensive contacts.

Following Ref. [43], we define the auto-correlation function (ACF) of ring-ring contacts via the contact number as follows

$$\mathrm{ACF}(\Delta) = \frac{\langle N_{AB}(t+\Delta) N_{AB}(t) \rangle - \langle N_{AB}(t+\Delta) \rangle \, \langle N_{AB}(t) \rangle}{\langle N_{AB}(t)^2 \rangle - \langle N_{AB}(t) \rangle^2}. \tag{7}$$

The averaging $\langle \ldots \rangle$ is performed over the times times t along the generated trace $N_{AB}(t)$ with the corresponding lag time Δ. The ACF characterises the decay of correlations in the overlap number of rings. The equilibration time in all our simulations is at least 50 times longer than the correlation time of the corresponding ACF for the inter-chain contact number for the chosen parameters.

An additional quantity characterising the ring-ring overlap is the relative position of their centres of mass,

$$\Delta z_{CM} = z_{CM,A} - z_{CM,B}. \tag{8}$$

From the corresponding probability density $p_{AB}(\Delta z_{CM})$ along the cylinder axis we compute the free energy of the overlap of the two rings in terms of

$$F(z_{CM}) = -k_B T \log[p_{AB}(z_{CM})] \tag{9}$$

in the Shannon sense.

3. Results

3.1. Dimensions and contacts of polymer rings

We verified that the extension of an unconfined ring polymer scales with its length as

$$\left\langle R_g^2(n) \right\rangle \sim n^{6/5}, \tag{10}$$

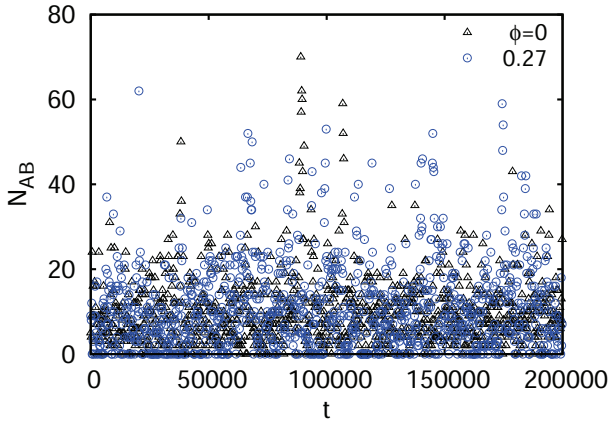

Figure 2. Fluctuations of the contact number $N_{AB}(t)$ of polymer rings as function of simulation time t, plotted for crowding fractions $\phi = 0$ and 0.27. Parameters: the number of monomers in each ring is $n = 200$, the radius of the confining cylinder is $R = 4.5\sigma$, the critical contact distance is $r_c = 1.5\sigma$, and the cylinder length is $L = 35\sigma$. Here and below the simulations time is presented in units of the time step δt.

consistent with the results reported in Ref. [45] (not shown). Our polymer rings are very flexible, the effective persistence length l_p being of the order of the monomer size (data not shown). Because of this extreme chain flexibility, we cannot analyse the implications of confinement onto the chain persistence (as compared to Ref. [38] where ring polymers were shown to stiffen substantially in tight confinement). Under the cylindrical confinement, the ring size $\langle R_g^2 \rangle$ naturally reaches a saturation for long chains. Once the chain dimensions overcome the size of the cylindrical cell, the polymer starts to folds on itself and its apparent scaling exponent ν decreases.

The initial ring configurations at $t = 0$ generated in the simulations are well-separated, positioned at the opposite sides of the confining cylinder. They exhibit a fast initial relaxation followed by a roughly exponential relaxation dynamics. At the later stages, when the polymers experience external confinement by the cylinder and the other ring, a non-exponential relaxation dynamics sets in. The spectrum of chain fluctuations in frequency space in the presence of external confinement and crowding becomes altered as well.

The general trend is that the instantaneous number of ring-ring contacts $N_{AB}(t)$ fluctuates strongly in the course of the simulations, compare Fig. 2. This trend is the same as in recent simulations for a similar system presented in the Supplementary Material of Ref. [43]. We observe that in the presence of crowders the ring-ring separation becomes more pronounced, and the probability density function PDF(N_{AB}) of their contact numbers exhibits a peak at $\langle N_{AB} \rangle = 0$. The spread of N_{AB} is slightly more localised in the presence of crowders, but both at crowded and non-crowded conditions the distributions $p(N_{AB})$ have long tails, as evidenced in Fig. 3 A. The relative centre-of-mass position of the two rings, Δz_{CM}, shows a larger spread in the

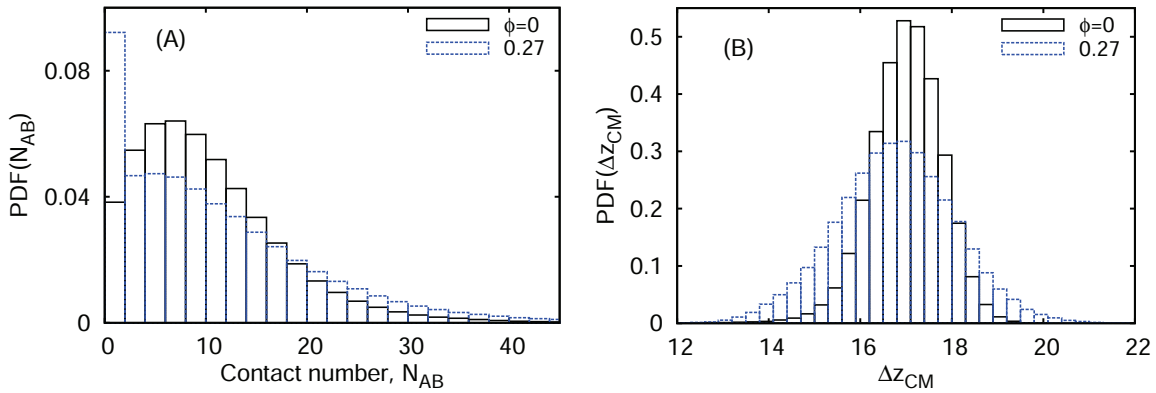

Figure 3. Probability density function of the ring-ring contact number (A) and centres of mass difference of the two rings (B), plotted for the parameters of Fig. 2.

presence of crowders, see Fig. 3B.

3.2. Ring swapping

For some choices of the volume and the aspect ratio of the confining cylinder as well as for shorter polymer lengths, the directed distance Δz_{CM} between the centres of mass of the two ring polymers exhibits clear alternations between two states while the rings are well separated near the ends of the confining cylinder, see Fig. 4. For such conditions, the diffusion times of the rings along the cylinder are relatively short, so they can pass one another and swap positions. At time instances when the rings are well separated the number of ring-ring contacts is minimal, while at almost vanishing centre of mass separation, $z_{CM} \sim 0$, the overlap of the rings is maximal and thus typically the $N_{AB}(t)$ traces are peaking at these instances, see the time series of $\Delta z_{CM}(t)$ and $N_{AB}(t)$ shown in Fig. 4. Note that the centre of mass distance $|\Delta z_{CM}| \leq L$, and the case of $\Delta z_{CM} > 0$ corresponds to the situation when ring A is located on the left half and ring B on the right half of the confining cylinder. This type of dynamics is reminiscent of the

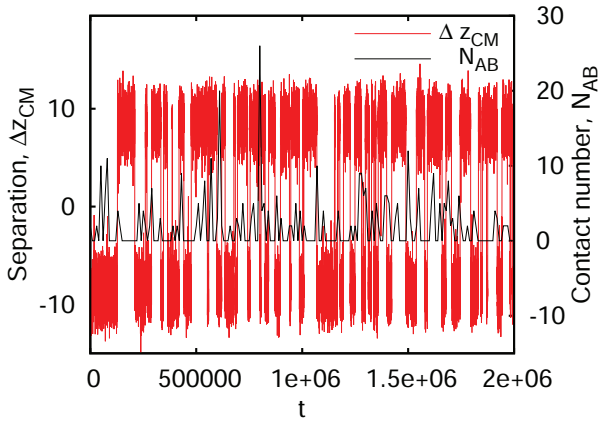

Figure 4. Time traces for the contact number $N_{AB}(t)$ (black) and the centre of mass distance of the rings Δz_{CM} (red). Every 10,000th and 100th data point is shown for the $N_{AB}(t)$ and $\Delta z_{CM}(t)$ trajectories, respectively. Parameters: no crowders ($\phi = 0$), chain lengths $n = 60$, cylinder radius $R = 5.5\sigma$ and length $L = 20\sigma$. A video illustrating the ring swapping events is included in the Supplementary Material.

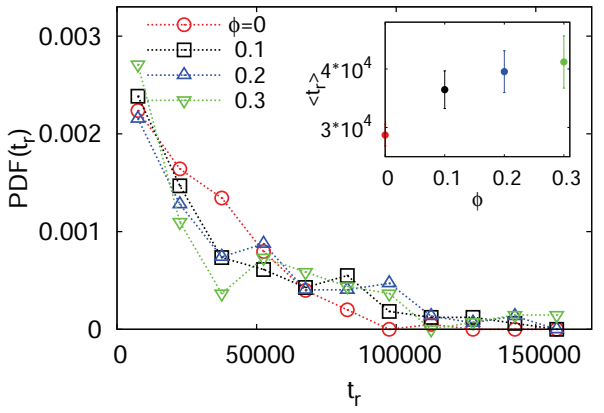

Figure 5. The distribution of the residence times t_r in the well-segregated ring states. The histograms are obtained from the zigzag traces similar to those presented in Fig. 4, but at varying crowding fractions. The inset shows the mean residence time of rings $\langle t_r \rangle$ in well-separated states as a function of ϕ.

periodic tumbling of polymers in shear flows, characterised by configurations with large extensions alternating with states of strong chain contraction, see, e.g., the studies reported in Refs. [67, 68].

For these conditions of well separated rings, the distribution of residence times t_r, that each ring is situated in one of the two well-separated states close to the cylinder ends, is shown in Fig. 5 for different crowding fractions ϕ. The mean residence time $\langle t_r \rangle$ extracted from these histogram is the characteristic time scale for the internal ring

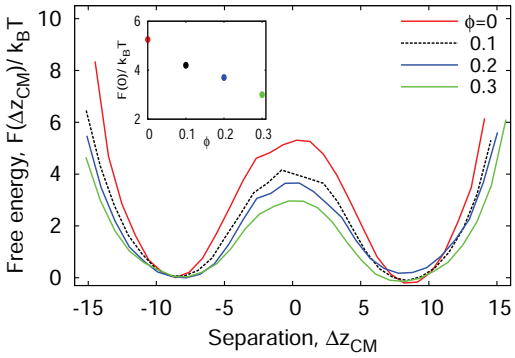

Figure 6. Double-well free energy landscape for ring swapping. The inset shows the magnitude of the free energy barrier for ring swapping computed at $\Delta z_{CM} = 0$. Parameters and notations for the curves are the same as in Fig. 5.

swapping dynamics. As shown in the inset of Fig. 5, $\langle t_r \rangle$ mildly increases with increasing ϕ. The maximum of the residence time histograms in Fig. 5 shifts at higher crowding fractions to larger values because of the associated slower polymer dynamics.

As illustrated in Fig. 6 the effective free energy for mixing the two rings has a double-well shape. The height of the barrier separating the two minimum states amounts to several k_BT for the parameters used in the simulations. As the residence times t_r in these separated ring states increases, the height of the free energy barrier between them decreases. This is due to a slower polymer dynamics at high crowding fractions, as discussed below. It also demonstrates that the free energy landscape is no true equilibrium measure, as known from the theory of polymer translocation [69].

Longer rings squeezed into the same confining cylinder reveal a slower swapping dynamics and the residence times in well-separated states grow until no swapping at all can be observed during the simulation time. Likewise, the exchange of rings in the simulation box is prohibited for smaller cylinder radii R (not shown).

3.3. Correlations of ring-ring contacts

As demonstrated in Fig. 2, the number of ring-ring contacts fluctuates strongly and irregularly. To find a typical time-scale for this variation, we compute the ACF (7) of the ring-ring contact number from the $N_{AB}(t)$ time traces. We start with the crowding-free case $\phi = 0$. The resulting curves in Fig. 7 show a fast relaxation at short times and turn to a nearly exponential decay at intermediate lag times Δ. At long times, the ACF drops to zero, indicating a complete loss of correlations. Some fluctuations of the ACF(Δ) at $\Delta \to \infty$ indicate insufficient statistics in the calculation of the time average (7). From Fig. 7, we observe that the initial decay of the ACF is slower for smaller cylinder radii, as expected. This is due to a larger space fraction in the simulation box being filled by the polymer monomers so that their motions get restricted to a larger

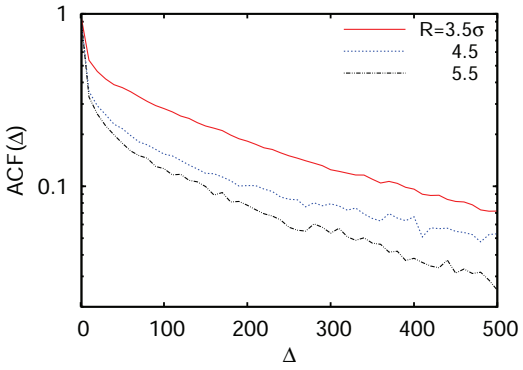

Figure 7. ACF of the ring-ring contact number N_{AB} defined in Eq. (7) in absence of crowders ($\phi = 0$) for different values R of the cylinder radius. Other parameters are the same as in Fig. 2.

extent, with many chains' moves being prohibited. For longer rings confined in the same cylinder, the ACF decays slower with the lag time Δ, again due to a smaller space available for the chains (not shown). Note that the intermediate-time decay exhibits comparable slopes in the logarithmic plot of Fig. 7.

3.4. Contacts and overlap of polymer rings: crowding effects

Let us now study the effects of the internal confinement due to crowding in more detail. We first consider a single ring polymer under the cylindrical confinement in the presence of crowding agents. The results for the mean squared gyration radius $\langle R_g^2 \rangle$ are shown in Fig. 8. We observe that the component of the radius of gyration measured along the cylinder axis is a slowly decreasing function of ϕ. Crowding particles thus act as a depletant, that effects ring shrinkage. For a less severe external confinement (larger cylinder radius R), we observe that the ring is more confined along the cylinder axis, but simultaneously more extended in the cylinder cross-section ($x - y$ plane), as shown in Fig. 8. Here we do not elaborate on the variation of the Flory scaling exponent ν of the gyration radius for a single ring as function of the external confinement and crowding (for such results see, e.g., the results reported in Ref. [46]). In the following we concentrate on the overlap properties of two polymer rings in the cylindrical simulations cell.

At higher fractions ϕ of crowders the correlation time of maintainig the established contacts between polymer rings increases due to the slower polymer dynamics, following a larger effective viscosity in a denser soup of crowders, i.e., the Rouse polymer dynamics becomes effectively slowed down by surrounding crowding particles. Concurrently, the same effect is responsible for a slower decay of the contact autocorrelations at higher values of ϕ, as shown in Fig. 9. The associated correlation time τ_C extracted from an

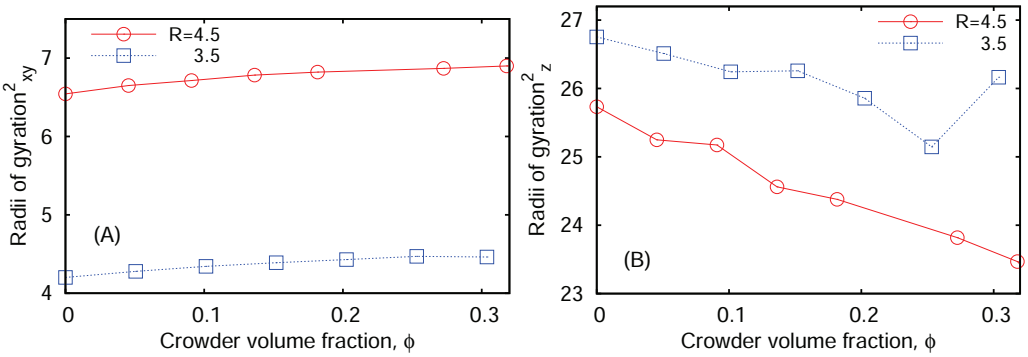

Figure 8. Mean squared gyration radius $\langle R_g^2 \rangle$ of a single polymer ring across the confining cylinder (A) and along (B) the cylinder axis, computed for varying crowding fractions ϕ and two different radii R of the cylinder. Other parameters are the same as in Fig. 2.

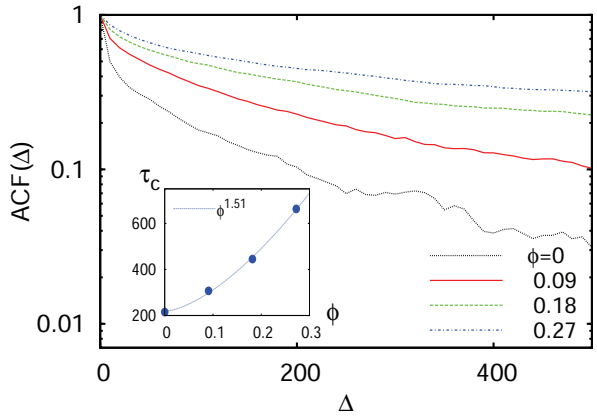

Figure 9. ACF function of ring-ring contacts, Eq. (7), for different crowding fractions ϕ and the parameters of Fig. 2. The inset shows the correlation time $\tau_C(\phi)$ determined from the decay $\exp(-\Delta/\tau_C)$ of the ACF(Δ) curves.

exponential fit of the ACF(Δ) curves exhibits the power-law dependence

$$\tau_C(\phi) \sim \phi^{3/2} \tag{11}$$

on the fraction of crowders, see the inset of Fig. 9. The 3/2 exponent indicates that the changes due to crowding are indeed a volume effect. Note that the single-ring relaxation time τ_R should not be confused with τ_C for the ring-ring contacts.

The dependence on the presence of mobile crowders on the three-dimensional contact characteristics and the effective one-dimensional overlap properties of polymer rings of fixed length are analysed in Fig. 10. We observe that the average number of ring-ring contacts $\langle N_{AB} \rangle$ increases significantly with the decrease of the cylinder radius R, i.e., when the chains are forced into a stronger contact by the external confinement, see Fig. 10A. As function of the internal confinement due to crowding, in some situations the number of ring-ring contacts N_{AB} exhibits a weakly non-monotonic dependence, see, e.g., the blue symbols in Fig. 10B. For weaker external confinement (larger R) we observe a mildly increasing dependence while it is decreasing for the smaller cylinder radius. This behaviour indicates a tradeoff between crowding and external confinement.

The effective overlap length of the rings along the cylinder axis is, in contrast, a very reproducible function with the functional relation

$$\langle l_{AB}(\phi) \rangle \approx \langle l_{AB}(0) \rangle \, (1 - \phi). \tag{12}$$

of the crowding fraction ϕ, compare Fig. 10A. This fact indicates a nearly ideal mixing of polymer monomers and crowding particles, as if the chain connectivity plays a minor role. The absolute values of l_{AB} for different cylinder radii vary only marginally. The decrease in Eq. (12) can be understood from a shrinkage of individual ring polymers by the crowders, as rationalised for longitudinal ring dimensions in Fig. 8B. We note a relatively small value of the overlap length at all crowding densities used in simulations. It is consistent with the results of Ref. [43] where, in the absence of crowders, a very limited inter-penetration and overlap of the two polymer rings was obtained.

We also systematically examined the effect of the contact distance r_c, defining the overlap of both polymer monomers and crowders, on the number of ring-ring contacts established in the simulations. We find that the average number of contacts naturally grows with r_c, compare Fig. 11. We also note that the error bars somewhat increase with ϕ and r_c but always stay smaller than the symbol size. Here and below, as proposed in Ref. [43], for the ring-ring contacts the error bars are computed with the blocking method introduced for correlated data sets in Ref. [70].

The statistical effects of the polymer-crowder mixing are analysed in terms of their distributions in the simulation cell. We find that for weak and moderate crowding fractions there is an accumulation of crowders near the cylinder ends, as evidenced in Fig. 12A. In turn, the polymer monomers are located preferentially off the middle of the cylinder, see Fig. 12B. We also observe that at small ϕ the crowding particles are effectively excluded from regions occupied by the polymers, thus facilitating ring-ring contacts. At stronger crowding, a peak of crowding particles in the middle of the

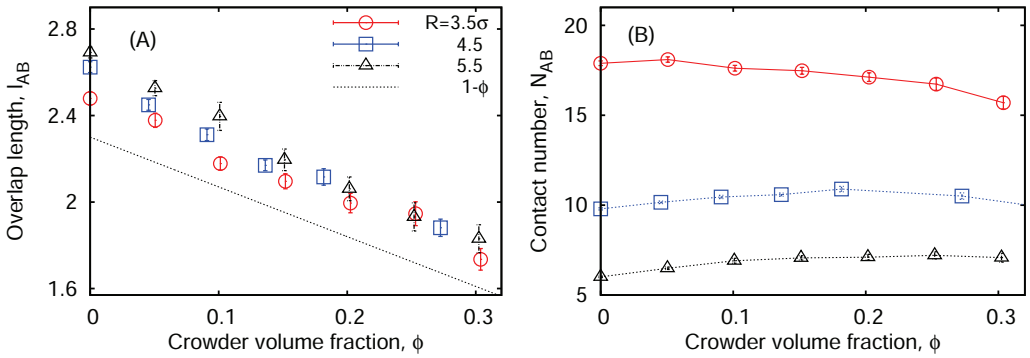

Figure 10. Average ring-ring overlap length along the cylinder axis (A) and average contact number (B), plotted for the parameters of Fig. 2.

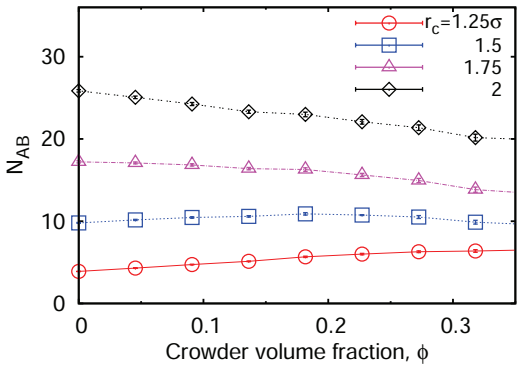

Figure 11. Average number of ring-ring contacts computed for varying contact distances r_c at cylinder radius $R = 4.5\sigma$. Other parameters are the same as in Fig. 2.

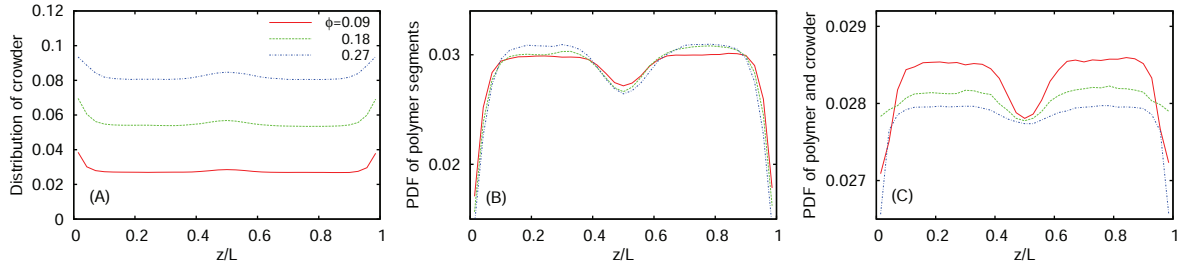

Figure 12. Distribution of crowding particles (A), polymer monomers (B), and the cumulative crowder-polymer distribution (C), plotted along the cylinder axis for varying ϕ fractions. Parameters are the same as in Fig. 2.

cell (between the polymer rings) emerges, see the blue curve in Fig. 12A. These mid-positioned crowding particles trigger an entropy-driven segregation of polymer rings, and their three-dimensional contact number N_{AB} decreases at larger ϕ values (Fig. 13B).

The mixing properties of polymers and crowders can be probed by the cumulative probability distribution of their monomers shown Fig. 12C. The decrease of $N_{AB}(\phi)$ at high ϕ is both due to a progressive emergence of crowders in between the polymers and a longitudinal shrinkage of each of the rings with ϕ. The ideal $(1-\phi)$ polymer-crowder mixing is realised at high ϕ, when the sum of the distributions of the polymer monomers and crowders is almost constant throughout the simulation cell, see Fig. 12C. Note that in order to sample the polymer configurations equally well at varying crowding fractions, longer simulation times are usually required at high ϕ values.

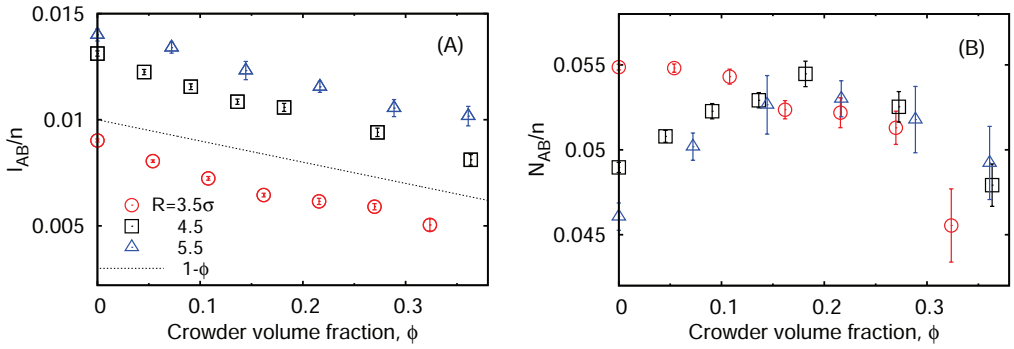

Figure 13. Relative overlap length (A) and contact number of polymer rings (B) in expanding simulation cells. In this figure the polymer volume fraction is kept constant at $\phi_p \approx 0.09$, and the length of the polymer rings is $n = 102$, 200, and 348 monomers for cylinder radii of $R = 3.5\sigma$, 4.5σ, 5.5σ, respectively. Note the larger deviations around the mean for the contact numbers N_{AB} at more crowded conditions (the error bars are computed by the blocking method [70]). The square symbols represent the same data set as in Fig. 10B for $R = 4.5\sigma$.

3.5. Variation of the polymer length

In the previous sections, most of the results presented were obtained for a constant polymer length of $n = 200$ monomers. To be able to scale up the our computations, we computed the ring-ring overlap length and contact number for longer polymers and larger simulation cells. The geometrical proportions of the confining cylinder, the aspect ratio R/L, were kept constant and at the same time the ring length was adjusted so the polymer volume fraction $\phi_p = V_p/V$ stays constant at $\phi_p \approx 0.09$. We observe that both the one-dimensional overlap length of the polymer rings and their three-dimensional contact number follow universal curves, after normalisation with respect to the number of monomers, i.e., for l_{AB}/n and N_{AB}/n. These results are illustrated in Fig. 13, which is the main result of this work. The ring-ring overlap length follows the $(1 - \phi)$-asymptote typical for the ideal mixing for all the parameters analysed in our simulations. In contrast, the number of contacts N_{AB} reveals a more delicate dependence. For small confining cylinders the contact number is a monotonically decreasing function

(red symbols in Fig. 13B). For larger simulation cells, the value of $N_{AB}(\phi)$ exhibits a maximum at $\phi \approx 0.2$ (black and blue symbols in Fig. 13B). This fraction $\phi \approx 20\%$ is reminiscent of the turning-point value for the non-monotonic dependencies on the fraction of crowding molecules mentioned in the Introduction, namely, of the dimensions of self-avoiding polymers [48] and diffusion-limited chemical reactions [49].

To compute l_{AB}/n and N_{AB}/n, we averaged over $M = 2 \times 10^5$, 2×10^5, and 8×10^4 simulation steps for cylinder radii $R = 3.5\sigma$, 4.5σ, 5.5σ, respectively. The simulation time on a standard 3-3.5 GHz core machine for each crowding fraction ϕ presented in Fig. 13 is about 2, 3, and 10 days, respectively. To accumulate reliable statistical information about the ring-ring contacts at relatively large crowding fractions, particularly long simulations are required because of the slower dynamics of inter-ring mixing. Last, at the same volume fraction of crowders ϕ, one can expect crowding particles of larger sizes to cause stronger effects on mixing properties of polymer rings.

4. Conclusions

Based on extensive Langevin dynamics simulations we analysed the behaviour of polymer chains of a circular topology in the presence of external confinement in a cylindrical geometry and internal crowding by molecular crowding agents. The size of the cylindrical confinement with respect to the monomer size and the length of the chains was chosen to represent the situation of two DNA rings in a typical bacillus cell. The crowding agents were represented by thermally agitated, off-lattice mono-disperse hard spheres. We found that the topological constraints restricting the polymer dynamics alter the response of partially intermingled circular polymers compared to linear chains. In highly crowded environments the polymer dynamics was demonstrated to be slowed down significantly. We found that high concentrations of crowding agents facilitate the spatial separation of ring polymers in cylindrical confinement. In addition, we quantified the extent to which the presence of crowding agents slows down the dynamics of the polymer-crowder system. The simulations for chains of varying length demonstrates that our model results are robust and in principle scalable to the dimensions of real bacterial cells.

The effect of molecular crowding obtained above are applicable to de-mixing of genome-sized DNA molecules inside bacterial cells as well as to the behaviour of relatively short DNA plasmids confined in natural compartments inside eukaryotic cells. The abundance of macromolecular crowders also offers a robust and non-specific way to tune the amount of DNA-DNA contacts. The dynamics and spatial occurrence of the latter are vital for biological processes such as DNA-DNA recognition and DNA homologous recombination [43], when the search for the homologous DNA partner in a coil of a long DNA is to be performed. Note that it would be interesting to analyse how the DNA-polymer segregation takes place in bacteria with other than rod-like shapes, such as in nearly planar squarish or spherical bacteria, see the discussion in Ref. [31].

The compartmentalisation of obstacles and polymer chains we observed can also

have implications for ageing phenomena of bacterial cells. For *E. Coli* cells, for instance, a localisation of age-related protein aggregates in low-crowding regions near the cell poles and in between of the two DNA nucleoids was observed. This effect was recently quantified by computer simulations at higher degrees of polymer and DNA crowding inside the nucleoids that hinder the diffusion of these protein aggregates [71].

Acknowledgments

JS thanks W. K. Kim for providing a computer code for analysis of ring swapping dynamics. The authors acknowledge funding from the Academy of Finland (FiDiPro scheme to RM), the German Research Council (DFG Grant CH 707/5-1 to AGC), and the German Federal Ministry for Education and Research (to JS).

References

[1] S. Jun and A. Wright, Nature Rev. Microbiol. **8**, 600 (2010).
[2] R. Hancock, PLoS ONE **7**, e36045 (2012).
[3] J. Dekker, A. Marti-Renom, and L. A. Mirny, Nature Rev. Genet. **14**, 390 (2013).
[4] T. B. K. Lee et al., Science **342**, 731 (2013).
[5] D. Bates and N. Kleckner, Cell **121**, 899 (2005).
[6] T. Cremer and C. Cremer, Nature Rev. Genet. **2**, 292 (2001).
[7] J. Dorier and A. Stasiak, Nucl. Acids Res. **37**, 6316 (2009).
[8] A. Rosa and R. Everaers, PLoS Comput. Biol. **4**, e1000153 (2008).
[9] A. Rosa, N. B. Becker and R. Everaers, Biophys. J. **98**, 2410 (2010).
[10] I. Bronstein, Y. Israel, E. Kepten, S. Mai, Y. Shav-Tal, E. Barkai, and Y. Garini, Phys. Rev. Lett. **103**, 018102 (2009).
[11] K. Kroy and J. Glaeser, New J. Phys. **9**, 416 (2007).
[12] D. Marenduzzo et al., Proc. Natl. Acad. Sci. U.S.A. **106**, 22269 (2009).
[13] G. Saper et al., Nucl. Acids Res. **41**, 1569 (2013).
[14] C. Zhang et al., Proc. Natl. Acad. Sci. U.S.A. **106**, 16651 (2009).
[15] S. B. Zimmerman and L. D. Murphy, FEBS Lett. **390**, 245 (1996).
[16] A. R. McGuffee and A. H. Elcock, PLoS Comp. Biol. **6**, e1000694 (2010).
[17] S. B. Zimmerman and A. P. Minton, Annu. Rev. Biophys. Biomol. Struct. **22**, 27 (1993).
[18] I. Goychuk, Adv. Chem. Phys. **150**, 187 (2012).
[19] J.-H. Jeon, H. Martinez-Seara Monne, M. Javanainen, and R. Metzler, Phys. Rev. Lett. **109**, 188103 (2012).
J-.H. Jeon, N. Leijnse, L. Oddershede, and R. Metzler, New J. Phys. **15**, 045011 (2013).
[20] E. Barkai, Y. Garini, and R. Metzler, Physics Today **65**(8), 29 (2012).
F. Höfling and T. Franosch, Rep. Prog. Phys. **76**, 046602 (2013).
[21] I. Golding and E. C. Cox, Phys. Rev. Lett. **96** 098102 (2006).
[22] S. C. Weber, A. J. Spakowitz, and J. A. Theriot, Phys. Rev. Lett. **104**, 238102 (2010).
[23] J. Szymanski and M. Weiss, Phys. Rev. Lett. **103**, 038102 (2009).
[24] J.-H. Jeon, V. Tejedor, S. Burov, E. Barkai, C. Selhuber-Unkel, K. Berg-Sørensen, L. Oddershede, and R. Metzler, Phys. Rev. Lett. **106**, 048103 (2011).
[25] S. M. A. Tabei, S. Burov, H. Y. Kim, A. Kuznetsov, T. Huynh, J. Jureller, L. H. Philipson, A. R. Dinner, and N. F. Scherer, Proc. Natl. Acad. Sci. USA **110**, 4911 (2013).
[26] H. X. Zhou, J. Mol. Recognit. **17**, 368 (2004).
[27] C. Echeverria and R. Kapral, Phys. Chem. Chem. Phys. **14**, 6755 (2012).

[28] C. A. Brackley, M. E. Cates, and D. Marenduzzo, Phys. Rev. Lett. **111**, 108101 (2013).
[29] O. Stiehl, K. Weidner-Hertrampf, and M. Weiss, New J. Phys. **15**, 113010 (2013).
[30] T. Kuhn et al., PLoS One **6**, e22962 (2011).
[31] S. Jun, "Polymer Physics for Understanding Bacterial Chromosomes", Chapter 6 in "Bacterial Chromatin", p. 97-116, Eds.: R. T. Dame and C. J. Dorman, Springer, (2010).
[32] S. Jun and B. Mulder, Proc. Natl. Acad. Sci. USA **103**, 12388 (2006), and references cited therein.
[33] R. Metzler, Y. Kantor, and M. Kardar, Phys. Rev. E **66**, 022102 (2002).
[34] M. Rubinstein, Phys. Rev. Lett. **57**, 3023 (1986).
[35] C. Micheletti and E. Orlandini, Macromol. **45**, 2113 (2012).
[36] L. Tubiana et al., Phys. Rev. Lett. **107**, 188302 (2011).
[37] C. Micheletti, D. Marenduzzo, and E. Orlandini, Phys. Rep. **504**, 1 (2011).
[38] Y. Jung et al., Soft Matter **8**, 2095 (2012).
[39] F. Benedetti, J. Dorier, Y. Burnier, and A. Stasiak, Nucl. Acids Res., at press; DOI:10.1093/nar/gkt1353.
[40] A. Narros et al., Macromol. **46**, 3654 (2013).
[41] S. Y. Reigh and D. Y. Yoon, ACS Macro Lett. **2**, 296 (2013).
[42] D. Racko and P. Cifra, J. Chem. Phys. **138**, 184904 (2013).
[43] J. Dorier and A. Stasiak, Nucl. Acids Res. **41**, 6808 (2013).
[44] D. Micheletti et al., arXiv:1306.4965
[45] E. Orlandini et al., Phys. Rev. E **82**, 050804(R) (2010).
[46] Two scaling regimes for ring dimensions were predicted in Ref. [45]. Namely, rings smaller than the lattice size b behave as a self-avoiding walk, $\langle R_g^2 \rangle \sim n^{1.15}$, while large rings follow the law for the branched polymers [G. Parisi and N. Sourlas, Phys. Rev. Lett. **46**, 871 (1981)]: $\langle R_g^2 \rangle \sim n^1$. Similarly, for knotted rings the dynamics turns from a self-avoiding walk to a branched polymer dynamics [45].
[47] J. S. Kim et al., Phys. Rev. Lett. **106**, 168102 (2011).
[48] J. S. Kim and I. Szleifer, J. Phys. Chem. C **114**, 20864 (2010).
[49] J. D. Schmit, E. Kamber, and J. Kondev, Phys. Rev. Lett. **102**, 218302 (2009).
[50] A. Marcovitz and Y. Levy, Biophys. J., **104** 2042 (2013).
[51] A. Gopinathan and Y. W. Kim, Phys. Rev. Lett. **99**, 228106 (2007).
[52] Y. Chen and K. Luo, J. Chem. Phys. **138**, 204903 (2013).
[53] A. Lappala, A. Zaccone, and E. M. Terentjev, Scientific Reports **3**, 3103 (2013).
[54] J. Shin, A. G. Cherstvy, and R. Metzler, work in preparation.
[55] J. Shin, A. G. Cherstvy, and R. Metzler, arXiv:1310.5531.
[56] V. V. Rybenkov, A. V. Vologodskii, and N. R. Cozzarelli, Nucl. Acids Res. **25**, 1412 (1997).
[57] A. R. McGuffee and A. H. Elcock, PLoS Comp. Biol. **6**, e1000694 (2010).
[58] J. T. Mika et al, Mol. Microbiol. **77**, 200 (2010).
[59] A. Savelyev, C. K. Materese, and G. A. Papoian, J. Am. Chem. Soc. **133**, 19290 (2011).
[60] A. G. Cherstvy, J. Biol. Phys. **37**, 227 (2011).
[61] A. G. Cherstvy, J. Phys. Chem. B **115**, 4286 (2011).
[62] T. Ando and J. Skolnick, Proc. Natl. Acad. Sci. U.S.A. **107**, 18457 (2010).
[63] H. H. Wensink et al., Proc. Natl. Acad. Sci. U.S.A. **109** 14308 (2012).
[64] G. A. Hegde et al., J. Chem. Phys. **135**, 184901 (2011).
[65] Y. Jung et al., Phys. Rev. E **79**, 061912 (2009).
[66] A. G. Cherstvy and V. B. Teif, J. Biol. Phys. **39**, 363 (2013).
[67] R. G. Winkler, Phys. Rev. Lett. **97**, 128301 (2006).
[68] C. C. Huang et al., J. Phys.: Cond. Matt. **24**, 284131 (2012).
[69] J. Chuang, Y. Kantor, and M. Kardar, Phys. Rev. E **65**, 011802 (2001).
K. Luo, T. Ala-Nissila, S.-C. Ying, and R. Metzler, Europhys. Lett. **88**, 68006 (2009).
[70] H. Flyvbjerg and H. G. Petersen, J. Chem. Phys. **91**, 461 (1989).
[71] A. S. Coquel et al, PLoS Comput. Biol. **9**, e1003038 (2013).